Long-Range Dynamic Effects of Point Mutations Propagate through Side Chains in the Serine Protease Inhibitor Eglin c†

Michael W. Clarkson‡ and Andrew L. Lee*,‡,§

Department of Biochemistry and Biophysics, School of Medicine, University of North Carolina, Chapel Hill, North Carolina 27599, and Division of Medicinal Chemistry and Natural Products, School of Pharmacy, University of North Carolina, Chapel Hill, North Carolina 27599

Received March 22, 2004; Revised Manuscript Received July 21, 2004

ABSTRACT: Long-range interactions are fundamental to protein behaviors such as cooperativity and allostery. In an attempt to understand the role protein flexibility plays in such interactions, the distribution of local fluctuations in a globular protein was monitored in response to localized, nonelectrostatic perturbations. Two valine-to-alanine mutations were introduced into the small serine protease inhibitor eglin c, and the ^{15}N and ^{2}H NMR spin relaxation properties of these variants were analyzed in terms of the Lipari−Szabo dynamics formalism and compared to those of the wild type. Significant changes in picosecond to nanosecond dynamics were observed in side chains located as much as 13 Å from the point of mutation. Additionally, those residues experiencing altered dynamics appear to form contiguous surfaces within the protein. In the case of V54A, the large-to-small mutation results in a rigidification of connected residues, even though this mutation decreases the global stability. These findings suggest that dynamic perturbations arising from single mutations may propagate away from the perturbed site through networks of interacting side chains. That this is observed in eglin c, a classically nonallosteric protein, suggests that such behavior will be observed in many, if not all, globular proteins. Differences in behavior between the two mutants suggest that dynamic responses will be context-dependent.

Protein stability and function are products of cooperative processes. Such processes occur in protein folding, ligand recognition, receptor signaling, enzyme catalysis, and multiprotein complex assembly. A major question in understanding cooperativity, and therefore function, in proteins is how residues separated by a distance influence or "sense" one another (*1*, *2*). Long-range communication has been frequently observed in proteins, although its origin is not always clear. In the widely studied allosteric mechanism of hemoglobin, long-range effects are brought about by conformational change (*3*). However, similar effects have been observed in proteins in the absence of obvious conformational changes (*4*−*9*), including instances of these effects that have appeared as a result of a single amino acid mutation (*6*, *7*, *10*). Hydrogen exchange studies have provided particularly striking examples of this behavior (*11*−*15*), suggesting that protein flexibility may play a role in propagated effects arising from localized perturbations.

Increasingly, experimental and theoretical studies have shown that both mutations and ligand binding can have consequences for protein motions at locations extending beyond the directly affected site, even in instances where structural changes are minimal. NMR-based experiments monitoring dynamics as a function of ligand binding in calmodulin (*16*), Cdc42 (*17*), an SH2 domain (*18*), and a PDZ domain (*19*) have shown significant effects on side-chain order parameters at sites up to 21 Å from the ligand-binding sites. Some of the results are precisely as expected: side chains at the interface between the protein and the ligand generally become more rigid upon binding, as one would predict simply from the sterics of the interaction. What has been somewhat surprising is that in all these cases the dynamic response to binding of the ligand is not necessarily limited to the binding interface, even though the majority of these proteins are not classical allosteric systems. Findings of this kind are not limited to ligand binding; experiments with protein L have revealed marked changes in methyl dynamics on the nanosecond time scale at sites distal to point mutations (*20*). Additionally, experiments with chymotrypsin inhibitor 2 revealed changes in the dynamics of a tryptophan side chain in response to an R → A mutation 13 Å away (*21*). Though these discoveries may seem to be somewhat startling, they have been preceded by findings in molecular dynamics simulations (*22*−*24*). From both experiment and theory, the biophysical evidence indicates that mutation and ligand binding can have far-reaching dynamic effects.

From MD simulations and normal-mode analysis, correlated motions or "dynamic coupling" has been proposed as a means for how dynamic effects might link sites separated by some distance (*23*−*26*). In principle, this would provide a physical, or mechanical, basis for energy transmission when obvious changes in conformation neither are apparent nor

† This research was supported by NIH Grant GM066009, the University of North Carolina Molecular and Cell Biophysics Training Program, and a seed grant from the Pharmacy Foundation of North Carolina, Inc.

* To whom correspondence should be addressed: Division of Medicinal Chemistry and Natural Products, School of Pharmacy, University of North Carolina, 310 Beard Hall, CB# 7360, Chapel Hill, NC 27599-7360. E-mail: drewlee@unc.edu. Phone: (919) 966-7821. Fax: (919) 843-5150.

‡ School of Medicine.

§ School of Pharmacy.

10.1021/bi0494424 CCC: $27.50
Published on Web 09/09/2004

provide a reasonable mechanism. In initial experimental work supporting this hypothesis, the propagation of motion in the PDZ and SH2 domains has been attributed to the existence of *dynamic networks* involving the affected residues (*18*, *19*). Precisely what these networks are, the rules by which they operate, and how they integrate with structural and energetic interactions within proteins have not yet been the subject of experimentation.

Dynamics experiments on backbone NH groups have consistently shown substantial rigidity in structured regions of the protein, suggesting that the main chain alone will not be efficient in transmitting motions through the protein. By contrast, order parameters (*27*) corresponding to the methyl 3-fold symmetry axis (S^2_{axis})[1] typically range from nearly 0 to more than 0.9, and while solvent-exposed methyl groups are flexible as expected, packing into the hydrophobic core of a protein does not necessarily confer rigidity (*28*−*31*). The parameter that best correlates with S^2_{axis} is the distance between the methyl group and the backbone (as this increases, the order parameter decreases). Recent experiments suggest that unusually high S^2_{axis} values (compared to averages for comparable methyl groups) have a modest correlation with sequence conservation (*32*), but it has been reported that correlations to structural parameters such as accessible surface area and packing density are weak at best (*30*). Accordingly, the determination of side-chain order parameters under a single condition is unlikely to provide any particular insight about a given protein's behavior. More insight may be gained, however, if the dynamics of the system are in some way disturbed: the reaction of the system could reveal the pathways of motional energy dispersion.

In an effort to understand how propagation occurs in proteins, we introduce here a dynamic perturbation-response experiment for the identification of dynamic networks. Site-specific changes in picosecond to nanosecond dynamics are monitored in response to a localized perturbation, in this case mutations. If the overall structural effects of the disturbance are not significant, one can reliably conclude that the residues reacting to the modified structure and motions at the mutation site belong to a dynamic network involving the perturbed residue. This mapping approach is demonstrated for two point mutations in the small serine protease inhibitor eglin c, the effects of which were analyzed in terms of model-free dynamics parameters for the backbone amides and methyl-bearing side chains. Simple criteria were applied to determine which residues experience a significant change in dynamics. The results indicate that the dynamic effects of a mutation propagate away from the perturbation site through networks of contiguous side chains. Of the two mutants that were studied (V14A and V54A), V54A results in a coherent rigidification of methyl-bearing residues, while V14A results in a smaller, mixed response.

[1] Abbreviations: ΔG_u, free energy change associated with two-state unfolding events; HSQC, heteronuclear single-quantum coherence; NMR, nuclear magnetic resonance; NOE, nuclear Overhauser effect; NOESY, nuclear Overhauser enhanced spectroscopy; PCR, polymerase chain reaction; RDC, residual dipolar coupling; S^2, Lipari−Szabo "model-free" generalized order parameter; S^2_{axis}, axial model-free order parameter for methyl groups; T_1, spin−lattice relaxation time constant; T_2, spin−spin relaxation time constant; τ_e, Lipari−Szabo model-free effective correlation time; τ_m, correlation time for overall tumbling; VDW, van der Waals.

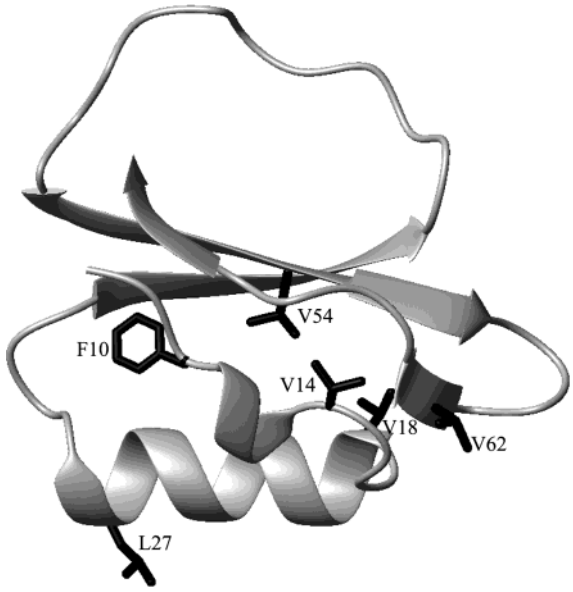

FIGURE 1: Serine protease inhibitor eglin c mutated at six sites (side chains shown). F10 was mutated to W in all proteins that were examined. Additionally, complete assignments and dynamics information were obtained for alanine mutations at V14 and V54. Thermodynamic unfolding data were obtained for alanine mutations at V18, V62, and L27, as well as V14A/V18A, V54A/L27A, and V54A/V62A double mutants. The structure is from a cocrystal with subtilisin Carlsberg (PDB entry 1cse) (*67*). This figure was created using MOLMOL (*68*).

EXPERIMENTAL PROCEDURES

Preparation of Mutant Proteins. All experiments were performed on the serine protease inhibitor eglin c (*33*) with an F10W mutation. This mutation has negligible effects on structure (unpublished data), and all other members of the potato inhibitor 1 family (to which eglin c belongs) have a W in this position. Accordingly, this mutant will be termed the wild-type (WT) for purposes of this study. Further mutations were made by site-directed mutagenic PCR. The sites of single mutations (V14A, V18A, L27A, V54A, and V62A) are shown in Figure 1. Additionally, V14A/V18A, L27A/V54A, and V54A/V62A double mutants were constructed. Mutant proteins were expressed in *Escherichia coli* BL21(DE3) cells and purified as previously described (*34*). NMR samples used in relaxation studies contained 2.0 mM eglin c in a standard buffer [20 mM KH_2PO_4, 50 mM KCl, 0.02% NaN_3, and 10% D_2O (pH 7.0)].

NMR Spectroscopy. NMR data were collected on 500 and 600 MHz Varian INOVA spectrometers equipped with triple-resonance probes at 37 °C (temperature calibrated with ethylene glycol). Spectra were processed using NMRPipe (*35*) and analyzed with the aid of NMRView (*36*). Complete assignments were compiled for WT, V14A, and V54A eglin c using samples uniformly labeled with ^{15}N and ^{13}C as previously described (*34*). Stereospecific methyl assignments were obtained using samples 10% labeled with ^{13}C and a standard constant-time HSQC spectrum (*37*).

One-bond $^{15}N-^{1}H$ dipolar couplings (*38*) were determined using 1 mM protein labeled 99% with ^{15}N, aligned in C12E5/hexanol bicelles (*39*). Couplings were obtained by comparing HSQC−IPAP experiments (*40*) performed at 500 MHz on the same sample at 20 °C (aligned) and 30 °C (unaligned). Alignment was confirmed using quadrupolar splitting of D_2O. Splittings were measured using NMRView (*36*). Bicelle solu-

tions for WT and V54A proteins were made from a single stock solution.

^{15}N relaxation data were collected on a sample labeled 99% with ^{15}N at both spectrometer fields using standard experiments (*41*) with slight modifications (*34*). ^{15}N T_1 data were collected with relaxation delays of 39, 109, 194, 299, 414, 544, 689, 839, and 1004 ms. $T_{1\rho}$ data were collected with delays of 5, 15, 25, 40, 60, 80, 105, and 135 ms at both fields, and spin-lock frequencies of 2518 Hz at 600 MHz and 2710 Hz at 500 MHz. Uniform uncertainties for all peak intensities were assessed using duplicate points (underlined delays above). {^{1}H}−^{15}N NOE data were collected with a ^{1}H saturation period of 4.5 s, and uncertainties were assessed from baseline noise. Peak intensities were extracted using NMRView and fitted to single-exponential decays using a Levinthal−Marquardt algorithm. $T_{1\rho}$ values were corrected for the offset-dependent T_1 contribution to the observed decay to yield pure T_2 values. Relaxation data were then fitted to the standard model-free formalism (*27*) using relxn2.1 (*42*) and an isotropic rotational diffusion tensor. τ_m values were determined by eliminating residues showing unusual flexibility (high T_1/T_2 ratio or NOE value of <0.65 at 600 MHz) and performing a global minimization of τ_m on the remaining residues (*43*).

Side-chain dynamics were assessed using samples uniformly labeled with ^{13}C and randomly 50% labeled with ^{2}H. ^{2}H spin relaxation data were collected at both 500 and 600 MHz, filtered for CH_2D methyl isotopomers using experiments previously described (*44*). $I_zC_zD_z$ delay times were 3.0, 7.4, 13.1, 19.9, 27.5, 34.0, 45.2, 55.0, and 65.6 ms. $I_zC_zD_y$ delay times were 1.1, 3.2, 5.8, 8.9, 12.4, 16.3, 20.5, 25.1, and 30.0 ms. I_zC_z values were collected with delays of 12, 20, 28, 36, 44, 52, 60, 68, and 76 ms. Uniform uncertainties for all peak intensities were assessed on the basis of duplicate measurements (underlined above). Relaxation times were fit using the same procedure that was used for backbone NH groups, and the pure D_z and D_y time constants were obtained as previously described (*44*). Relaxation data were best-fitted to the standard model-free formalism, and S^2 values were divided by a factor of 0.111 to correct for methyl rotation (*27*, *44*).

Chemical Denaturation. ΔG_u values were determined using protocols already described for eglin c mutants (*45*). Briefly, samples of ~5 μM protein in NMR buffer (without D_2O) were titrated with a solution with an equal protein concentration containing 6.8 M guanidine hydrochloride. Titrations were performed with an automatic titrating fluorimeter at 25 °C, and unfolding was monitored by fluorescent emission from W10 at 350 nm (excitation wavelength of 290 nm). Denaturant curves were fit and ΔG_u values obtained as previously described (*45*). $\Delta\Delta\Delta G_i$ values were obtained by subtracting the sum of $\Delta\Delta G_u$ values for the single mutants from the $\Delta\Delta G_u$ value for the double mutant. Chemical denaturation experiments were performed in quadruplicate for WT, V14A, V18A, V54A, V62A, V14A/V18A, and V54A/V62A, and in duplicate for L27A and V54A/L27A. The observed precision was similar to that of previous experiments (*45*).

RESULTS

Structure of Eglin c Mutants. V14A and V54A mutants were chosen to characterize the effect of mutations on the dynamics of eglin c. These mutants are destabilized by 1.04 and 1.58 kcal/mol (Table 1), respectively, relative to WT (ΔG_u = 6.05 ± 0.08 kcal/mol at 25 °C). V14 lies at the C-terminal end of the short 3^{10}-helix and is partially solvent-exposed (Figure 1). V54 is positioned in the middle of strand 3 of the large β-sheet, with its side chain pointing directly into the hydrophobic core. Both mutants and the WT protein are stable at room temperature and at 37 °C for more than 2 weeks. All mutants yielded disperse ^{15}N−^{1}H HSQC spectra with sharp peaks, and complete assignments of WT, V14A, and V54A proteins proceeded using routine procedures (*46*). The chemical shifts of the fully assigned mutants (V14A and V54A) were compared to those of WT to determine whether significant structural rearrangement had occurred. Assessments of amide chemical shifts in which the contributions of proton and nitrogen are scaled by their gyromagnetic ratios indicate that most of the structural perturbations are local in nature, generally extending only to residues that are spatially or sequentially adjacent. Neither mutant has residues that experience a significant change in both S^2_{axis} and ^{1}H/^{15}N chemical shift, except for residues adjacent to the mutation site (e.g., V13 in V14A). A secondary structure analysis was also performed, on the basis of C^α, H^α, and C^β chemical shifts. Though slight changes in these shifts result from the mutations, they are consistent with unchanged secondary structure. Additionally, direct comparison of one-bond ^{15}N−^{1}H residual dipolar couplings between WT and V54A isoforms (Figure 2) revealed a strong linear correlation (R^2 = 0.986). This provides strong evidence that the tertiary structure of eglin c is unchanged by the mutations.

Table 1: Free Energies of Unfolding at 25 °C for Mutants Determined by Chemical Denaturation Using GuHCl

mutant	$\Delta\Delta G_u$[a]	$\Delta\Delta\Delta G_i$[a,b]
V14A	−1.038 ± 0.111	−
V18A	−1.203 ± 0.140	−
L27A	−0.161 ± 0.118	−
V54A	−1.579 ± 0.154	−
V62A	−1.014 ± 0.085	−
V14A/V18A	−2.519 ± 0.171	−0.279 ± 0.247
L27A/V54A	−1.970 ± 0.163	−0.230 ± 0.253
V54A/V62A	−2.867 ± 0.216	−0.274 ± 0.279

[a] $\Delta\Delta G_u$ values are in kilocalories per mole, relative to the WT protein. [b] $\Delta\Delta\Delta G_i$ values are the value of the double mutant minus the sum of the values of the single mutants.

Rotational Correlation Times. Backbone NH dynamics and global tumbling were characterized from ^{15}N T_1, T_2, and {^{1}H}−^{15}N NOE relaxation (*47*). Global fits of the rotational correlation time τ_m are in agreement between the mutant proteins (4.64 ns for both) and WT (4.68 ns). Relaxation data from each protein fit well to an isotropic rotational diffusion tensor, and attempts to fit the data to axially symmetric oblate or prolate tensors using N−H vectors obtained from the 25 eglin c solution structures determined by Hyberts *et al*. (PDB entry 1egl) (*48*) resulted in nearly identical parallel and perpendicular components ($D_\parallel/D_\perp$ = 1.05 ± 0.10, 1.09 ± 0.05, and 1.04 ± 0.06 for WT, V14A, and V54A, respectively). When model-free parameters were determined using independent fits of τ_m for individual bond vectors (*49*), narrow τ_m distributions (4.63 ± 0.2 ns for V14A, 4.65 ± 0.2 ns for V54A, and 4.69 ± 0.2 ns for WT) were found in structured regions of the proteins. Fits of

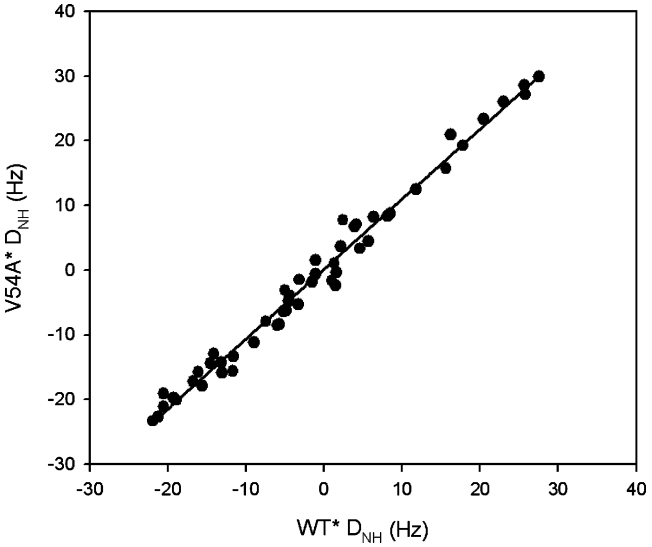

FIGURE 2: One-bond $^{15}N-^{1}H$ dipolar couplings plotted for the WT protein against the V54A protein. The line is from a linear fit of the data that yielded a correlation coefficient R of 0.992 ($R^2 = 0.985$).

internal model-free parameters proceeded using the τ_m determined for each individual protein.

Backbone Model-Free Parameter Comparison. Order parameters for backbone NH vectors were determined from ^{15}N spin relaxation measurements performed at two fields. Those determined for WT (Figure 3) are typical for a folded protein and closely match order parameters previously determined for eglin c at pH 3.0 (*50*). Backbone order parameters are generally high (>0.8) except in the region of the flexible protease-binding loop, and $\langle S^2 \rangle$ for WT is approximately 0.82 in structured regions. Comparison of NH order parameters between each mutant and WT indicates no significant changes of flexibility as a result of mutation (Figure 4). The $\langle |\Delta S^2| \rangle$ of residues for which order parameters could be determined was 0.01 ± 0.01 for comparisons of either V14A or V54A with WT. Microsecond to millisecond conformational exchange processes detected at residues 13 and 66, and in the binding loop (residues 39−41, 44, and 48), did not appear to be affected by any mutations.

While there are several residues that can be identified as undergoing significant changes in backbone dynamics using the criteria outlined below for side chains, the vast majority of these changes are marginal effects on scale with the noise, and few of the changes appear to make structural sense. Affected residues appear to be dispersed throughout the protein with no discernible pattern or connectivity.

Side-Chain Model-Free Parameter Comparison. The picosecond to nanosecond motions of side chains were determined for methyl CH_2D isotopomers using ^{2}H spin relaxation measurements at two fields, followed by fitting to model-free parameters S^2 and τ_e. Correction of these order parameters for methyl rotation yields S^2_{axis} values describing the motion of the axial methyl C−C bond (*27*, *44*). Order parameters determined for WT reveal a greater degree of both flexibility and heterogeneity than backbone values; this is typical for a folded protein (*29*−*31*). Comparisons of model-free parameters between mutant proteins and WT indicate that in each mutant, significant changes in $S_{axis}{}^2$ are restricted to a limited number of residues.

Residues identified as undergoing a significant change in dynamics are those for which either $|\Delta S^2_{axis}|$ or $|\Delta \tau_e|$ is more than twice the uncertainty determined for those difference values. Several residues in each mutant met this qualification (Figure 5) (for purposes of comparison, an alternate standard of 3 times the error was also used; see the Supporting Information). In the V14A mutant, V13, T17, and V18 were all identified as changing significantly. Additionally, V34 and L45 were identified as changing, though they were only 0.001 above the threshold. Because of intermediate exchange behavior at L45 and because of unusually high χ^2 values associated with model-free fits of its methyls, L45 was excluded from the response network on the assumption that the dynamics model was not appropriate. In the case of V34, however, all available data suggest that the Lipari−Szabo formalism is adequate for describing the dynamics. Accordingly, we regard the V34 response as real, though not with a high level of confidence.

The responses to mutation are even more extensive in the V54A mutant: residues V13, T17, V18, A21, V34, V52, and V62 all met the criteria for "change", though with V52 only one of the two methyls showed changes above the threshold. Additionally, the changes for both V13 and T17 are small (Figure 5).

In both mutants, nearly all the affected residues form contiguous surfaces. In the case of V14A, a combination of increases and decreases in S^2_{axis} is observed. By contrast, the V54A mutation causes only increases in S^2_{axis}, which may be viewed as a concerted rigidification of side chains. This picosecond to nanosecond rigidification accompanies a global free energy *destabilization* of 1.58 kcal/mol (Table 1; see below).

It is important to note that in both mutants a significant number of residues did not experience any appreciable change in picosecond to nanosecond side-chain dynamics. This indicates that the observed changes are not due to errors in the calculated τ_m. Even small errors in the determination of the correlation time can produce substantial changes in fitted S^2_{axis} and τ_e values. However, these changes are expected to be global and uniform in sign (though the magnitude would be scaled by the actual S^2_{axis} value), and as such would be noticeable at nearly all side chains. The absence of this effect does not guarantee an accurate τ_m for the reference state (WT), but it strongly suggests that the $\Delta \tau_m$ between states is correct.

Thermodynamic Coupling Free Energy Analysis. In an attempt to determine whether residues with a common dynamic response to a perturbation also share free energy, thermodynamic mutant cycle analysis (*51*, *52*) was performed using the ΔG of unfolding (ΔG_u) as a probe of interaction. To avoid complications from the contribution of shared VDW surfaces (*53*, *54*), the secondary mutations were introduced at residues (V18 and V62) not in contact with the primary mutation sites (V14 and V54, respectively). In addition, a thermodynamic mutant cycle was constructed between V54 and L27, as a negative control. The results, summarized in Table 1 for 25 °C, show that although the individual mutations have the expected effects on protein stability, i.e., destabilization, the interaction of noncontacting residues does not make a measurable energetic contribution to the free energy difference between the native and de-

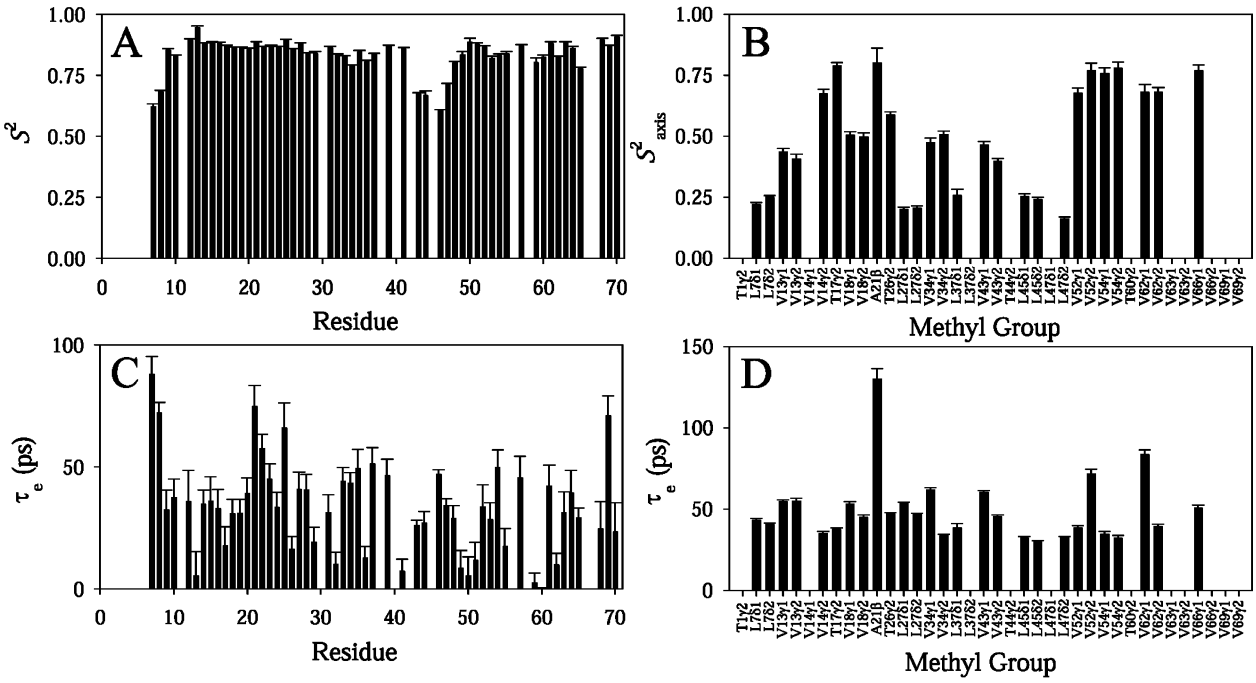

FIGURE 3: Model-free dynamics parameters determined for the WT protein. Backbone NH S^2 (A) and τ_e (C) values determined from ^{15}N relaxation were similar to those previously described for eglin c at pH 3. The highly dynamic N-terminus did not yield distinct peaks at pH 7. Side-chain S^2_{axis} (B) and τ_e (D) values determined from ^2H relaxation matched typical patterns for folded proteins.

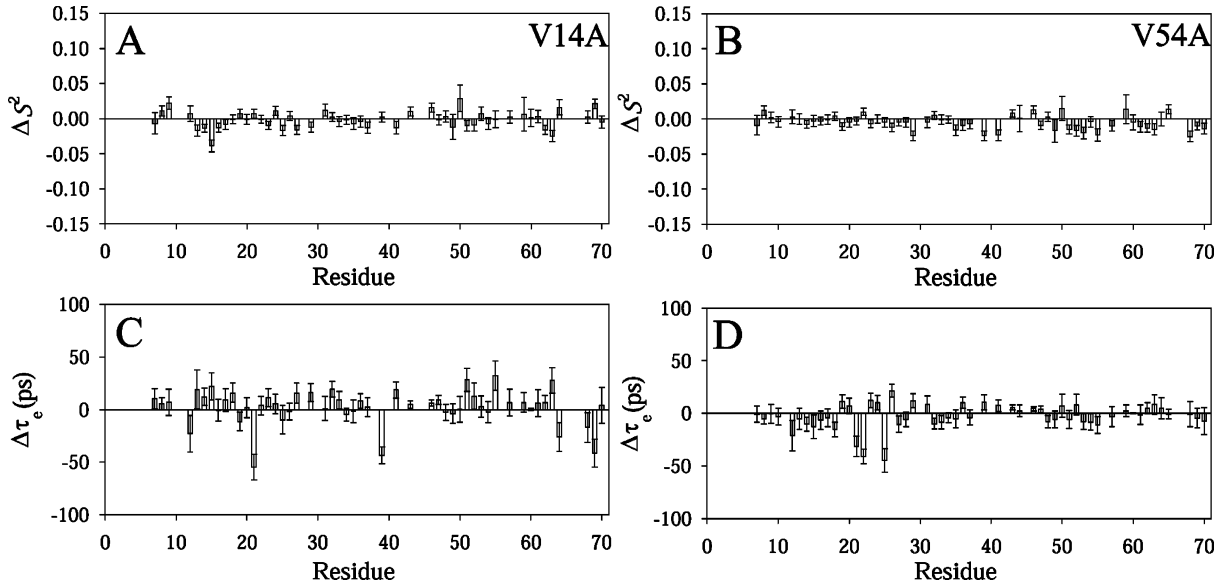

FIGURE 4: Differences in backbone NH model-free dynamics parameters for eglin c mutants. All values are the mutant value minus the WT value. ΔS^2 (A and B) and $\Delta\tau_e$ (C and D) values are shown for V14A (A and C) and V54A (B and D) mutants.

natured states. Additional experiments on the V54/V62 thermodynamic cycle at 37 °C confirm that the coupling free energy is essentially 0 over a range of temperatures (data not shown).

DISCUSSION

Dynamic Effects of Mutation Propagate through Side-Chain Networks. We show here a novel, NMR-based approach for identifying dynamic networks that extend beyond a residue's first shell of packing interactions. Through monitoring side-chain motion via ^2H spin relaxation, the dynamic perturbation-response method has identified differential side-chain flexibilities for multiple residues as a result of point mutations to eglin c. The effects of single-amino acid substitutions V14A and V54A clearly extend far beyond the point of mutation in both cases (Figure 5). In addition, the dynamic responses are different in the two cases, highlighted by complete rigidification of side chains in V54A, in contrast to a mixture of increased and decreased flexibility in V14A. These results are consistent with conclusions from previous studies that mutational effects are context-dependent (*55*, *56*). Here, the positions of the mutations are in different structural contexts: V14A is partially solvent exposed (solvent-accessible surface area of 60.6 Å^2), whereas V54 points directly into the hydrophobic core and is fully buried.

Dynamical Response in V14A. The V14A mutation induces small but measurable changes in the picosecond to nano-

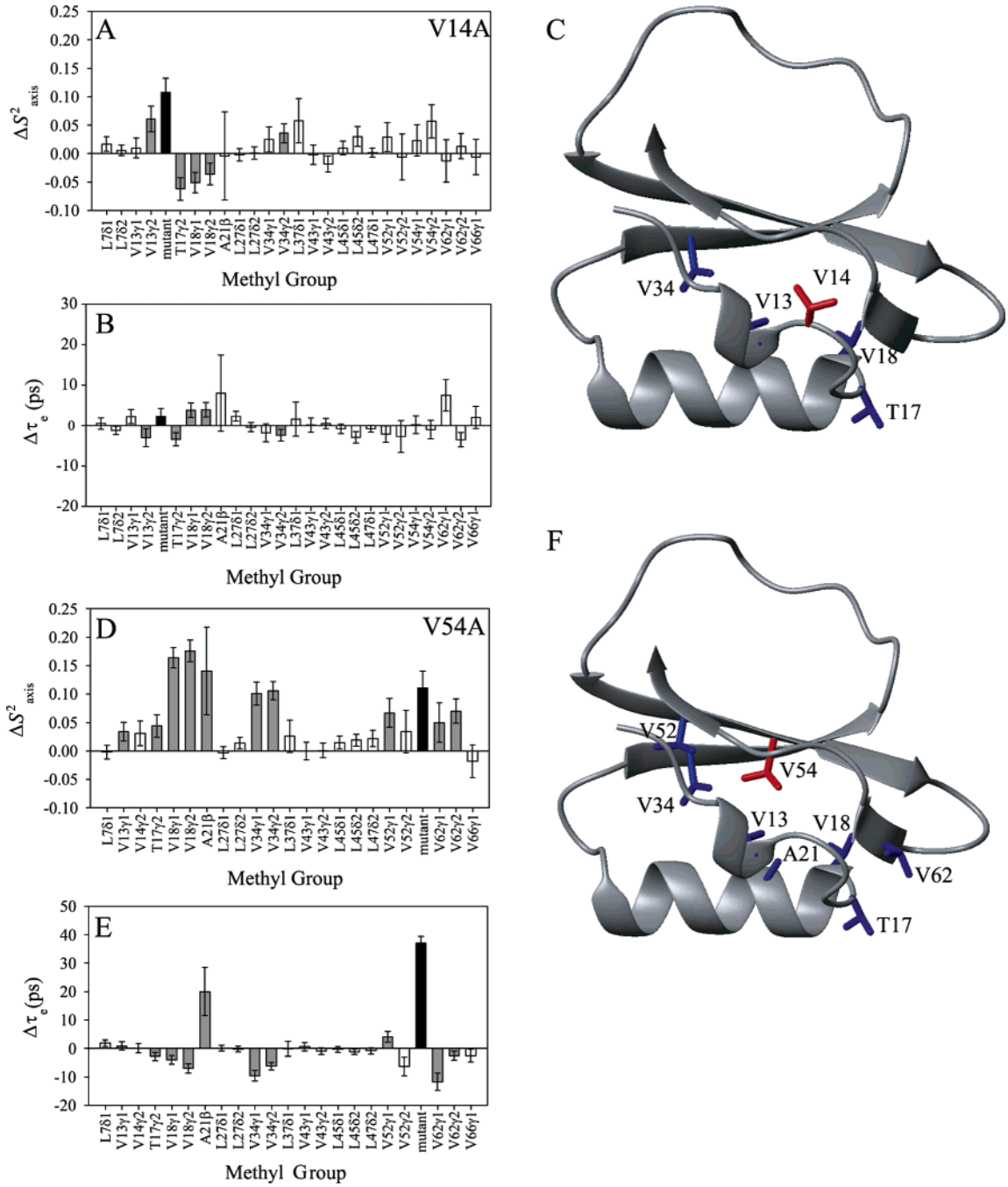

FIGURE 5: Differences in side-chain model-free dynamics parameters for eglin c mutants. All values are the mutant value minus the WT value. ΔS^2_{axis} (A and D) and $\Delta \tau_e$ (B and E) values are shown for V14A (A−C) and V54A (D−F) mutants, respectively. Side chains with significantly altered dynamics (as defined by a significance threshold; see the text) have shaded bars in graphs and are also depicted graphically in the context of the protease-bound eglin c structure (C and F) (*67*). Mutated residues have black bars in graphs and are red in the structural diagrams. Note that due to overlap it was not possible to determine order parameters for all methyls in all mutants. Protein images were created with MOLMOL (*68*).

second side-chain motions of residues that are connected by a series of van der Waals contacts, thereby forming a spatially coherent response to the mutation (Figures 5A−C and 6A). The methyl carbons of V18 and T17 are ~11 Å from the β-carbon of V14 (distances are almost 13 Å with the V14 methyls as the reference point). In addition, the V34 methyl carbons are more than 13 Å from the V14 β-carbon. Therefore, a seemingly insignificant mutation near the surface of the protein is sensed in two separate distal regions, showing that any given site may be influenced by distal residues that are not apparent from structural considerations. Though ΔS^2_{axis} and $\Delta \tau_e$ values are relatively small for V14A, their connective traceability from V14 reinforces their significance.

In the interpretation of NMR-based, dynamic perturbation-response experiments, two practical issues arise that relate to assessing the contiguity of residues. First, although the dynamics of a large number of side chains can be characterized, certain types of side chains will escape detection. Such missing information can leave apparent gaps in the propagated dynamic response. For example, in this study the dynamics of aromatic and methylene groups were not

measured. In addition, some methyl groups could not be analyzed due to signal overlap, which happens to be the case for both V63 methyls in WT eglin c. V63 is in the hydrophobic core and is in partial contact with both V14 and V54 (in WT eglin c). Because of this proximity of V63 to the mutated sites and its central position in both response pathways, we have considered it to be part of both dynamic networks and have highlighted it in Figure 6. Thus, in the case of V14A, propagated dynamical changes to V18 and T17 are likely to be mediated by V63. Similarly, propagation to V34 (left side of the structure) is likely to be mediated by F25, which bridges V13 and V34. The dynamic perturbation of V34 is almost undetectable, which may result from an inefficiency of an aromatic group to transmit motional perturbations. While buried phenylalanine and tyrosine side chains typically flip 180° on a sub-millisecond time scale, their bulkiness and inherent rigidity are expected to result in low mobility on time scales faster than tens of nanoseconds, which may serve to deflect propagated effects rather than promote them. Nevertheless, slight dynamic changes are observed at V34, so F25 is shown "on-path" in Figure 6A.

The second practical issue is that it is possible that some residues may be initially identified as part of the dynamic network (e.g., using our criteria for significant changes in ΔS^2_{axis} and $\Delta\tau_e$), even though they have no clear connection to it. This occurs with L45 in V14A. However, in that instance, other data strongly suggest dynamic complexity beyond the scope of the Lipari−Szabo formalism used here. Similarly, the alternate standard (Figure 1 of the Supporting Information) identified only T17 as a member of the network in the V14A mutant; in that case, the primary standard indicates an obvious pathway. Nonetheless, it is feasible that mutational effects may reach truly distant residues that cannot be connected from a contiguous path of perturbed dynamics. In these cases, "silent" energetic propagation may occur, and the structural and dynamical changes may be too subtle to detect. The absence of detectable dynamical changes (on this time scale) does not preclude propagation through any site.

Dynamical Response in V54A. The dynamical changes in response to the V54A mutation are more dramatic (Figure 5) than in the V14A mutant. This is most evident in the ΔS^2_{axis} values, which are as high as 0.2, although the distances between the mutation site and most of the affected residues are shorter than for V14A. Nonetheless, methyl groups of T17 and V62 are greater than 11 Å from the β-carbon of V54, and a contiguous pathway is observed that extends from V54 to these solvent-exposed positions (Figure 5). As found in V14A, V63 appears to mediate the dynamic propagation toward T17 and V62 by virtue of occupying a central position on the response pathway. Aside from the magnitude and mapping of the response, one other characteristic of V54A stands out: all side chains in the response pathway show an increase in rigidity. This concurrent rigidification of eight side chains (A54 included) in response to mutation is a separate, albeit perhaps related, indication of the coherence and collectivity of the response.

Though fewer side chains are identified as being perturbed using the alternate standard, the general characteristics of the pathway remain much the same. Only V63 needs to be added to connect all residues that are identified as experiencing dynamic perturbation into a contiguous network. In neither this mutant nor V14A does use of the alternate, more stringent standard significantly alter the conclusion that mutations have dynamic effects on distal residues, though in the case of V14A the response pathway becomes more difficult to map.

Models for Propagation of Changes in Picosecond to Nanosecond Dynamics. The observed patterns of changes in side-chain dynamics suggest a possible model for the dispersion of dynamic effects through the protein structure: networks of adjacent side chains transmit changes in forces and motion. In this simple model, side chains on the network must be in van der Waals contact and could be considered to have fluidlike or springlike properties to facilitate transmission. However, in these mutants, relatively rigid residues appear to be affected as well as relatively fluid ones, making it difficult to explain why the dynamic effects of these mutations are limited, rather than pervasive, or why different mutations excite different networks. This is significant, as there is mounting evidence that intramolecular, energetic networks in a wide variety of proteins are sparsely distributed throughout their structures (*57*). In the experiments shown here, V54 does not respond to V14A and V14 does not respond to V54A. Additionally, though both networks extend through V63, V18, and T17, the ΔS^2_{axis} values in V18 and T17 are opposite in sign: V14A mobilizes V18, whereas V54A restricts its mobility. Simple geometric analysis of the protein is not sufficient to explain these observations; therefore, dynamic networks must depend on more than mere adjacency.

More powerful models for explaining the mutant data can be based on motional modes and, hence, correlated motions. Much experimental and theoretical work has addressed correlated motions on backbone and side-chain atoms (*22*, *58*−*60*). Unfortunately, due to the nature of the relaxation measurements made here, S^2_{axis} values alone provide no information about the temporal correlation of motions of neighboring residues. In principle, if groups of side-chain bond vectors are moving synchronously, they should give rise to similar τ_e values (for a $C-CH_3$ bond). However, ^{2}H-derived τ_e values of methyl groups are convolutions of the residence times of methyl rotation and methyl axis diffusion, and deconvolution into the two components is not straightforward (*42*). Nevertheless, the contiguity of the residues involved in each network, and the fact that ΔS^2_{axis} has the same sign for most adjacent residues, is suggestive of a mechanism wherein fluctuations that are correlated in the WT protein, producing subglobal motional modes, are collectively affected by mutation. The coexistence of multiple modes may explain the different dynamic responses for V14A and V54A, as these two perturbations may differentially affect specific modes.

Finally, it may be that the effects of these two mutations, despite their similarities, reflect two fundamentally distinct dynamic responses. The surfaces in Figure 6 do not show many of the side chains of eglin c for purposes of clarity. Numerous aromatic side chains are present in the core, and while it is conceivable, particularly in light of the picosecond to nanosecond rigidity of buried aromatic side chains, that the observed dynamic effects are propagated solely by methyl-bearing residues, it is unrealistic to expect that this

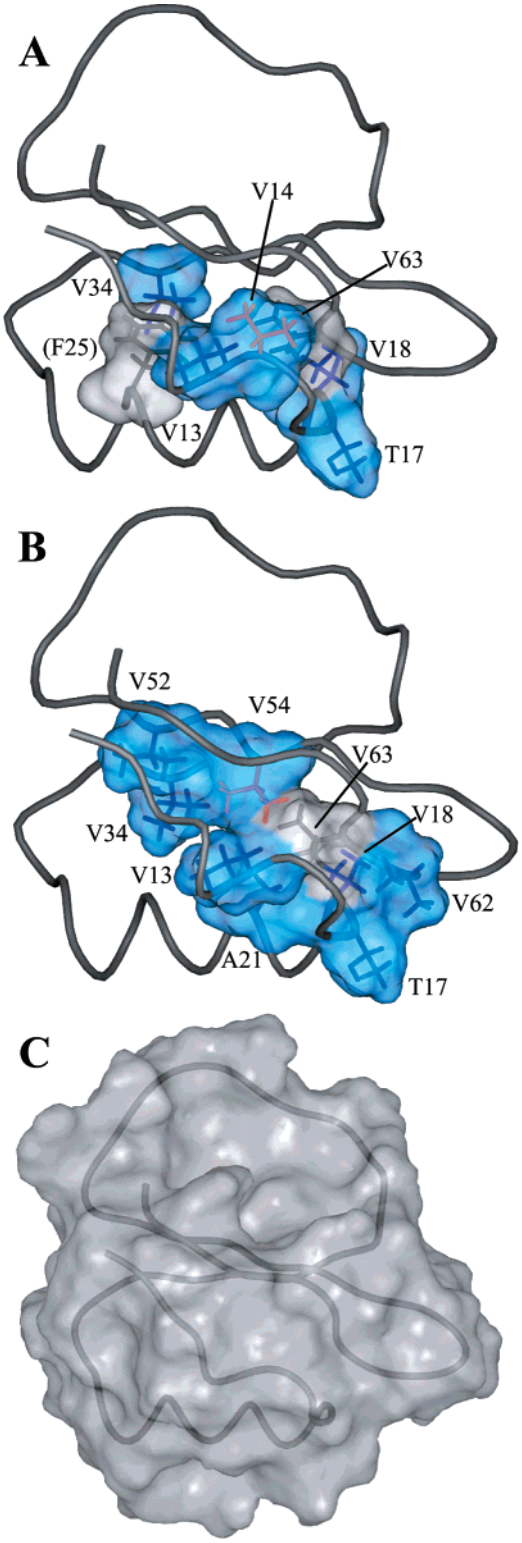

FIGURE 6: Diagram of side-chain surfaces involved in the eglin c response to mutations V14A (A) and V54A (B), and a full solvent-accessible surface diagram of eglin c (C). Surfaces were created using a probe with a radius of 1.4 Å in SPOCK (*69*). Residues not experiencing significantly altered motion are not depicted, with the exceptions of V63 (A and B) and F25 (A) (see the Discussion); the side chains of these residues and their associated surfaces are shown in gray. Mutated side chains are shown in red. The view in panel B is rotated slightly to display the network more clearly. Although the residues that are drawn are included on the basis of side-chain dynamics responses, corresponding backbone atoms are also included in the surface calculations. Note that although the loop is flexible and moves with considerable freedom, it is connected to the core by contiguous side-chain contacts.

is so. More likely, the aromatic side chains also rigidify in response to the V54A mutation, reflecting a generalized stiffening of core residues. Under this interpretation, outward-pointing residues V62 and T17 are merely experiencing transmission across the backbone from their more severely affected (and core-directed) neighbors. The V14A results, however, are *not* consistent with a hypothesis that the whole core is affected. In this case, we observe a more discrete network with two arms (of which one appears to be weaker) that experience different consequences. The dynamic effects may be passed across the backbone to V13 in such a way that it and V34 rigidify, while the other side of the network becomes more dynamic in an outcome mediated mostly by side-chain transmission. It should be emphasized that the dynamic transmission across the backbone mentioned above need not involve a significant change in backbone dynamics; indeed, none of the above cases involve such a change. In these circumstances, the backbone may be acting as a pivot for motion, or silent propagation may be occurring.

Absence of Significant Structural Change. It is tempting to ascribe the observed changes in order parameters solely to changes in dynamic processes. Support for this position comes from the RDC data (Figure 2); one-bond $^{15}N-^{1}H$ dipolar couplings do not differ substantially between the WT and V54A proteins, strongly suggesting that no significant changes in backbone conformation have occurred. The chemical shift data, as well as preliminary solution structures of V54A and WT, are consistent with this interpretation. Certainly, the existing data do not support a model that includes a drastic rearrangement of side-chain contacts as an explanation of the observed effects.

Nonetheless, even high-resolution structures may not be sufficiently accurate to rule out all rearrangements of side chains. Crystallographic and NMR structures do not capture the entire structural ensemble, but rather identify its lowest-energy and average members, respectively. Subtle changes in mean side-chain positions or the populations of particular conformers may therefore elude detection. As such, the observed networks may not only reflect altered motions of the protein but also serve as a probe of small structural effects not readily investigated by standard means. Such effects could be small shifts in side-chain positions (and their associated dynamical changes) or, alternatively, changes in methyl geometry (*27*).

Energetics of Dynamic Interactions. Residues that interact in terms of dynamics are almost certainly experiencing an energetic interaction, and the study of thermodynamic double-mutant cycles is a classic way of identifying such relationships (*51*−*53*). Provided that the interaction energy produces a measurable effect on protein behavior, a mutant cycle testing that thermodynamic behavior could identify the amino acids that are involved. The ΔG_u values determined in this study did not reveal any interaction free energy in the case of either dynamic network, at least not to the degree where the free energy was any greater than in the control L27A/V54A cycle with no dynamic interaction. This is consistent with previous experiments in which residues that appeared to have linked dynamics on the time scale of hydrogen exchange showed no measurable free energy interaction (*13*). These results may reflect a true absence of energetic interaction, or merely that the thermodynamic property studied (unfolding free energy) is not an appropriate

probe. Other properties (protease inhibition, folding kinetics, or heat capacity) may be affected by the dynamic network, and such properties will be targets of future studies. It is also possible that the energies involved with these fluctuations are too small to be measured reliably; if so, it may be that the combination of numerous interactions has a significant impact.

These findings may also reveal a limitation of the mutant cycle experiment itself, in that one cannot substitute a side chain smaller than alanine without introducing undesired structural and dynamic complications into the backbone. If all that is required to maintain the dynamic interaction is a C^{β}, then mutation to alanine will not disrupt it. Particularly in the case of V62, in which the methyls are directed *away* from the mutation site, the motional effects probably propagate through the interior carbons (C^{α} and C^{β}). Further studies are necessary to fully assess the energetic consequences of dynamic linkage in these networks.

Rigidity Does Not Imply Stability in V54A. It is natural to associate the concept of conformational stability with that of rigidity (*61*). Large structural fluctuations usually signify that the various interactions present in the primary conformation are energetically insufficient to maintain it. Thus, as the conformational space condenses toward a single structure, one naturally assumes that the stability of that structure has increased. While most of the observations with regard to the V14A mutation agree with this expectation, the observations of the V54A mutant do not (Figure 5 and Table 1). A substantial increase in rigidity in the V54A mutant accompanies a *loss* of stability. These experiments do not directly address side chain motions slower than the time scale of picoseconds to tens of nanoseconds, and clearly the protein *has* become more flexible on the time scale of global unfolding events. With the exception of global unfolding, however, it is reasonable to conclude that the fast motions describe a general effect in the native state.

Though these observations contradict common (perhaps macroscopic) intuitions about the relationship between stability and rigidity, they can be rationalized in thermodynamic terms. The increased rigidity of the side chains following the V54A mutation reflects a decrease in conformational entropy, though the possibility of correlated motions prevents a straightforward quantification of this effect (*31*, *62*). When viewed in this context, the rigidification of eglin c can be explained as a cause of its destabilization. This is consistent with previous work on WT eglin c, in which a pH drop (effectively neutralizing charge on all acidic residues) resulted in concurrent rigidification of multiple core methyl groups and loss of stability (*34*). In cases such as these, it may be useful to conceive of macromolecular instability in terms of *fragility* in the native state rather than in terms of a loose or fluctuating structure.

That a "cavity" mutation should cause a generalized rigidification of adjacent residues (as in V54A) also seems to be counterintuitive. However, the physical origins of side-chain flexibility remain so poorly understood that little can be definitively said about this result, except that it reemphasizes the already well-known disjuncture between packing quality and side-chain rigidity (*30*).

Dynamic Perturbation Response. Mutation has long been used as a tool for probing molecular behavior, and this and other studies (*20*, *21*, *60*) extend its use into the realm of dynamics. Recent studies with protein G have demonstrated that a series of surface mutations can be used as a probe of related backbone motions (*60*). The technique described therein uses mutation as an indirect probe of the networks that supposedly mediate motional correlation. By contrast, the dynamic perturbation-response method described here aims to directly identify the side chains involved in motion transmission by means of a single mutational disruption. The data from these experiments therefore serve complementary functions: probing the larger motions themselves and the mechanism whereby they are supposedly communicated. This approach has an advantage in that it directly probes the side chains, which may, as shown here, undergo significant changes in motion in the absence of any noticeable effect on the backbone (as detected at NH sites).

At present, it is not clear what significance the magnitude of a given change in S^2_{axis} has in terms of molecular behavior, particularly in light of the fact that there is as yet no good physical explanation of the determinants of side-chain order parameters. Rather than make a possibly flawed interpretation of the relative *degree* of change, here we intend only to determine which residues are connected to the perturbation site based upon a motional response following a mutation. The group of residues identified by the experiment constitutes a *dynamic network* (or subnetwork), providing a framework for further interpretation. That such extensive responses are observed in a small, classically rigid protein like eglin c suggests that more widespread and complex networks remain to be found in larger domains. It is important to note that these experiments may not have identified even the full extent of these networks; the relaxation of methylene groups was not fully characterized, nor were the effects on flip rates of aromatic residues (of which there are a large number in the core of eglin c) determined.

Of additional importance is the finding that mutations that have apparently small effects on structure and backbone dynamics may nonetheless have significant consequences for the motion of the side chains. As side chains constitute the primary tools proteins use for catalysis and ligand binding, nonlocal effects of this kind may be somewhat important in understanding the behavior of protein−protein interaction modules and enzymes, particularly in cases where single mutations have significant consequences for activity in the absence of apparent structural change (*10*). Though we could not determine the energy of the interactions detected here, it may be that the sum of many small interactions across a protein has major consequences for its behavior.

Explanations of allosteric effects have typically addressed only an interconversion between principal conformations of proteins, paradoxically both highlighting and ignoring their fundamental flexibility. While shifts in structure have often been acknowledged as the origin of a given allosteric behavior, fluctuations *around* a particular mean structure have generally been ignored as a possible cause. Nonetheless, the possibility of allostery without conformational change has been established from at least a theoretical perspective (*63*), and allosteric and cooperative behaviors have been observed in single-domain proteins where the classic structural explanations may not apply (*64*−*66*). In light of results presented here and elsewhere (*19*), it is reasonable

to ask whether conformational dynamics are responsible for some of these observations, and whether internal networks play a role.

ACKNOWLEDGMENT

We thank Greg Young and Fang Yi for their invaluable technical assistance. We further thank Hao Hu, Marshall Edgell, and Jan Hermans for fruitful theoretical discussion.

SUPPORTING INFORMATION AVAILABLE

A reproduction of Figure 5 using three standard deviations as the criterion for significant changes in S^2_{axis} and τ_e values. This material is available free of charge via the Internet at http://pubs.acs.org.

REFERENCES

1. Yu, E. W., and Koshland, D. E., Jr. (2001) Propagating conformational changes over long (and short) distances in proteins, *Proc. Natl. Acad. Sci. U.S.A. 98*, 9517−9520.
2. Luque, I., Leavitt, S. A., and Freire, E. (2002) The linkage between protein folding and functional cooperativity: Two sides of the same coin? *Annu. Rev. Biophys. Biomol. Struct. 31*, 235−256.
3. Perutz, M. F. (1970) Stereochemistry of cooperative effects in haemoglobin, *Nature 228*, 726−739.
4. Mace, J. E., Wilk, B. J., and Agard, D. A. (1995) Functional linkage between the active-site of α-lytic protease and distant regions of structure: scanning alanine mutagenesis of a surface loop affects activity and substrate-specificity, *J. Mol. Biol. 251*, 116−134.
5. McElroy, C., Manfredo, A., Wendt, A., Gollnick, P., and Foster, M. (2002) TROSY-NMR studies of the 91 kDa TRAP protein reveal allosteric control of a gene regulatory protein by ligand-altered flexibility, *J. Mol. Biol. 323*, 463−573.
6. Meroueh, S. O., Roblin, P., Golemi, D., Maveyraud, L., Vakulenko, S. B., Zhang, Y., Samama, J. P., and Mobashery, S. (2002) Molecular dynamics at the root of expansion of function in the M69L inhibitor-resistant TEM *β*-lactamase from *Escherichia coli*, *J. Am. Chem. Soc. 124*, 9422−9430.
7. Rajagopalan, P. T. R., Lutz, S., and Benkovic, S. J. (2002) Coupling interactions of distal residues enhance dihydrofolate reductase catalysis: Mutational effects on hydride transfer rates, *Biochemistry 41*, 12618−12628.
8. Muzammil, S., Ross, P., and Freire, E. (2003) A major role for a set of non-active site mutations in the development of HIV-1 protease drug resistance, *Biochemistry 42*, 631−638.
9. Ohtaka, H., Schon, A., and Freire, E. (2003) Multidrug resistance to HIV-1 protease inhibition requires cooperative coupling between distal mutations, *Biochemistry 42*, 13659−13666.
10. Howell, E. E., Booth, C., Farnum, M., Kraut, J., and Warren, M. S. (1990) A 2nd-site mutation at phenylalanine-137 that increases catalytic efficiency in the mutant aspartate-27 → serine *Escherichia coli* dihydrofolate reductase, *Biochemistry 29*, 8561−8569.
11. DeLorimier, R., Hellinga, H. W., and Spicer, L. D. (1996) NMR studies of structure, hydrogen exchange, and main-chain dynamics in a disrupted-core mutant of thioredoxin, *Protein Sci. 5*, 2552−2565.
12. Williams, D. C., Benjamin, D. C., Poljak, R. J., and Rule, G. S. (1996) Global changes in amide hydrogen exchange rates for a protein antigen in complex with three different antibodies, *J. Mol. Biol. 257*, 866−876.
13. Spudich, G., Lorenz, S., and Marqusee, S. (2002) Propagation of a single destabilizing mutation throughout the *Escherichia coli* ribonuclease HI native state, *Protein Sci. 11*, 522−528.
14. Anand, G. S., Hughes, C. A., Jones, J. M., Taylor, S. S., and Komives, E. A. (2002) Amide H/^{2}H exchange reveals communication between the cAMP and catalytic subunit-binding sites in the R′α subunit of protein kinase A, *J. Mol. Biol. 323*, 377−386.
15. Casares, S., Sadqi, M., Lopez-Mayorga, O., Martinez, J. C., and Conejero-Lara, F. (2003) Structural cooperativity in the SH3 domain studied by site-directed mutagenesis and amide hydrogen exchange, *FEBS Lett. 539*, 125−130.
16. Lee, A. L., Kinnear, S. A., and Wand, A. J. (2000) Redistribution and loss of side chain entropy upon formation of a calmodulin-peptide complex, *Nat. Struct. Biol. 7*, 72−77.
17. Loh, A. P., Pawley, N., Nicholson, L. K., and Oswald, R. E. (2001) An increase in side chain entropy facilitates effector binding: NMR characterization of the side chain methyl group dynamics is Cdc42Hs, *Biochemistry 40*, 4590−4600.
18. Finerty, P. J., Muhandiram, R., and Forman-Kay, J. D. (2002) Side-chain dynamics of the SAP SH2 domain correlate with a binding hot spot and a region with conformational plasticity, *J. Mol. Biol. 322*, 605−620.
19. Fuentes, E. J., Der, C. J., and Lee, A. L. (2004) Ligand-dependent dynamics and intramolecular signaling in a PDZ domain, *J. Mol. Biol. 335*, 1105−1115.
20. Millet, O., Mittermaier, A., Baker, D., and Kay, L. E. (2003) The effects of mutations on motions of side-chains in protein L studied by ^{2}H NMR dynamics and scalar couplings, *J. Mol. Biol. 329*, 551−563.
21. Leatherbarrow, R. J., and Matthews, S. J. (1992) Carbon-13 nuclear magnetic resonance relaxation study of chymotrypsin inhibitor-2 (CI-2), *Magn. Reson. Chem. 30*, 1255−1260.
22. Ichiye, T., and Karplus, M. (1991) Collective motions in proteins: a covariance analysis of atomic fluctuations in molecular dynamics and normal mode simulations, *Proteins 11*, 205−217.
23. Radkiewicz, J. L., and Brooks, C. L. (2000) Protein dynamics in enzymatic catalysis: Exploration of dihydrofolate reductase, *J. Am. Chem. Soc. 122*, 225−231.
24. Ceruso, M. A., Grottesi, A., and DiNola, A. (2003) Dynamic effects of mutations within two loops of cytochrome c_{551} from *Pseudomonas aeruginosa*, *Proteins 50*, 222−229.
25. Young, M. A., Gonfloni, S., Superti-Furga, G., Roux, B., and Kuriyan, J. (2001) Dynamic coupling between the SH2 and SH3 domains of c-Src and Hck underlies their inactivation by C-terminal tyrosine phosphorylation, *Cell 105*, 115−126.
26. Showalter, S. A., and Hall, K. B. (2002) A functional role for correlated motion in the N-terminal RNA-binding domain of human U1A protein, *J. Mol. Biol. 322*, 533−542.
27. Lipari, G., and Szabo, A. (1982) Model-Free Approach to the Interpretation of Nuclear Magnetic Resonance Relaxation in Macromolecules: 1. Theory and Range of Validity, *J. Am. Chem. Soc. 104*, 4546−4559.
28. Constantine, K. L., Friedrichs, M. S., Wittekind, M., Jamil, H., Chu, C. H., Parker, R. A., Goldfarb, V., Mueller, L., and Farmer, B. T. (1998) Backbone and side chain dynamics of uncomplexed human adipocyte and muscle fatty acid-binding proteins, *Biochemistry 37*, 7965−7980.
29. Johnson, E. C., and Handel, T. M. (1999) Effect of hydrophobic core packing on sidechain dynamics, *J. Biomol. NMR 15*, 135−143.
30. Mittermaier, A., Kay, L. E., and Forman-Kay, J. D. (1999) Analysis of deuterium relaxation-derived methyl axis order parameters and correlation with local structure, *J. Biomol. NMR 13*, 181−185.
31. Wand, A. J. (2001) Dynamic activation of protein function: a view emerging from NMR spectroscopy, *Nat. Struct. Biol. 8*, 926−931.
32. Mittermaier, A., Davidson, A. R., and Kay, L. E. (2003) Correlation between ^{2}H NMR side-chain order parameters and sequence conservation in globular proteins, *J. Am. Chem. Soc. 125*, 9004−9005.
33. Seemuller, U., Meier, M., Ohlsson, K., Muller, H. P., and Fritz, H. (1977) Isolation and characterisation of a low molecular weight inhibitor (of chymotrypsin and human granulocytic elastase and cathepsin G) from leeches, *Hoppe-Seyler's Z. Physiol. Chem. 358*, 1105−1117.
34. Hu, H., Clarkson, M. W., Hermans, J., and Lee, A. L. (2003) Increased rigidity of eglin c at acidic pH: Evidence from NMR spin relaxation and MD simulations, *Biochemistry 42*, 13856−13868.
35. Delaglio, F., Grzesiek, S., Vuister, G. W., Zhu, G., Pfeifer, J., and Bax, A. (1995) NMRPipe: a multidimensional spectral processing system based on unix pipes, *J. Biomol. NMR 6*, 277−293.
36. Johnson, B. A., and Blevins, R. A. (1994) NMRView: A computer program for the visualization and analysis of NMR data, *J. Biomol. NMR 4*, 603−614.
37. Neri, D., Szyperski, T., Otting, G., Senn, H., and Wuthrich, K. (1989) Stereospecific nuclear magnetic-resonance assignments of the methyl-groups of valine and leucine in the DNA-binding

domain of the 434-repressor by biosynthetically directed fractional C-13 labeling, *Biochemistry 28*, 7510−7516.
38. Tjandra, N., and Bax, A. (1997) Direct Measurement of Distances and Angles in Biomolecules by NMR in a Dilute Liquid Crystalline Medium, *Science 278*, 1111−1114.
39. Ruckert, M., and Otting, G. (2000) Alignment of Biological Macromolecules in Novel Nonionic Liquid Crystalline Media for NMR Experiments, *J. Am. Chem. Soc. 122*, 7793−7797.
40. Ottiger, M., Delaglio, F., and Bax, A. (1998) Measurement of *J* and Dipolar Couplings from Simplified Two-Dimensional NMR Spectra, *J. Magn. Reson. 131*, 373−378.
41. Farrow, N. A., Muhandiram, R., Singer, A. U., Pascal, S. M., Kay, C. M., Gish, G., Shoelson, S. E., Pawson, T., Forman-Kay, J. D., and Kay, L. E. (1994) Backbone dynamics of a free and phosphopeptide-complexed Src homology 2 domain studied by ^{15}N NMR relaxation, *Biochemistry 33*, 5984−6003.
42. Lee, A. L., Flynn, P. F., and Wand, A. J. (1999) Comparison of ^{2}H and ^{13}C NMR relaxation techniques for the study of protein methyl group dynamics in solution, *J. Am. Chem. Soc. 121*, 2891−2902.
43. Dellwo, M. J., and Wand, A. J. (1989) Model-independent and model-dependent analysis of the global and internal dynamics of cyclosporin A, *J. Am. Chem. Soc. 111*, 4571−4578.
44. Muhandiram, D. R., Yamazaki, T., Sykes, B. D., and Kay, L. E. (1995) Measurement of ^{2}H T_1 and $T_{1\rho}$ relaxation times in uniformly ^{13}C-labeled and fractionally ^{2}H-labeled proteins in solution, *J. Am. Chem. Soc. 117*, 11536−11544.
45. Edgell, M. H., Sims, D. A., Pielak, G. J., and Yi, F. (2003) High-precision, high-throughput stability determinations facilitated by robotics and a semiautomated titrating fluorometer, *Biochemistry 42*, 7587−7593.
46. Bax, A., and Grzesiek, S. (1993) Methodological advances in protein NMR, *Acc. Chem. Res. 26*, 131−138.
47. Palmer, A. G. (2001) NMR probes of molecular dynamics: Overview and comparison with other techniques, *Annu. Rev. Biophys. Biomol. Struct. 30*, 129−155.
48. Hyberts, S. G., Goldberg, M. S., Havel, T. F., and Wagner, G. (1992) The solution structure of eglin-c based on measurements of many NOEs and coupling-constants and its comparison with x-ray structures, *Protein Sci. 1*, 736−751.
49. Lee, L. K., Rance, M., Chazin, W. J., and Palmer, A. G. (1997) Rotational diffusion anisotropy of proteins from simultaneous analysis of ^{15}N and ^{13}C$^{\alpha}$ nuclear spin relaxation, *J. Biomol. NMR 9*, 287−298.
50. Peng, J. W., and Wagner, G. (1992) Mapping the spectral densities of N-H bond motions in eglin c using heteronuclear relaxation experiments, *Biochemistry 31*, 8571−8586.
51. Ackers, G. K., and Smith, F. R. (1985) Effects of site-specific amino-acid modification on protein interactions and biological function, *Annu. Rev. Biochem. 54*, 597−629.
52. Horovitz, A., and Fersht, A. R. (1990) Strategy for analysing the co-operativity of intramolecular interactions in peptides and proteins, *J. Mol. Biol. 214*, 613−617.
53. LiCata, V. J., and Ackers, G. K. (1995) Long-range, small magnitude nonadditivity of mutational effects in proteins, *Biochemistry 34*, 3133−3139.
54. Chen, J., and Stites, W. E. (2001) Energetics of side chain packing in staphylococcal nuclease assessed by systematic double mutant cycles, *Biochemistry 40*, 14004−14011.
55. Minor, D. L., and Kim, P. S. (1994) Context is a major determinant of β-sheet propensity, *Nature 371*, 264−267.
56. Cota, E., Hamill, S. J., Fowler, S. B., and Clarke, J. (2000) Two proteins with the same structure respond very differently to mutation: The role of plasticity in protein stability, *J. Mol. Biol. 302*, 713−725.
57. Suel, G. M., Lockless, S. W., Wall, M. A., and Ranganathan, R. (2003) Evolutionarily conserved networks of residues mediate allosteric communication in protein, *Nat. Struct. Biol. 10*, 59−69.
58. Miller, D. W., and Agard, D. A. (1999) Enzyme specificity under dynamic control: a normal mode analysis of α-lytic protease, *J. Mol. Biol. 286*, 267−278.
59. LeMaster, D. M. (1999) NMR relaxation order parameter analysis of the dynamics of protein side chains, *J. Am. Chem. Soc. 121*, 1726−1742.
60. Mayer, K. L., Earley, M. R., Gupta, S., Pichumani, K., Regan, L., and Stone, M. J. (2003) Covariation of backbone motion throughout a small protein domain, *Nat. Struct. Biol. 10*, 962−965.
61. Wray, J. W., Baase, W. A., Lindstrom, J. D., Weaver, L. H., Poteete, A. R., and Matthews, B. W. (1999) Structural analysis of a non-contiguous second-site revertant in T4 lysozyme shows that increasing the rigidity of a protein can enhance its stability, *J. Mol. Biol. 292*, 1111−1120.
62. Lee, A. L., Sharp, K. A., Kranz, J. K., Song, X. J., and Wand, A. J. (2002) Temperature dependence of the internal dynamics of a calmodulin-peptide complex, *Biochemistry 41*, 13814−13825.
63. Cooper, A., and Dryden, D. T. F. (1984) Allostery without conformational change: a plausible model, *Eur. Biophys. J. 11*, 103−109.
64. Rostovtseva, T. K., Liu, T.-T., Colombini, M., Parsegian, V. A., and Bezrukov, S. M. (2000) Positive cooperativity without domains or subunits in a monomeric membrane channel, *Proc. Natl. Acad. Sci. U.S.A. 97*, 7819−7822.
65. Frauenfelder, H., McMahon, B. H., Austin, R. H., Chu, K., and Groves, J. T. (2001) The role of structure, energy landscape, dynamics, and allostery in the enzymatic function of myoglobin, *Proc. Natl. Acad. Sci. U.S.A. 98*, 2370−2374.
66. Volkman, B. F., Lipson, D., Wemmer, D. E., and Kern, D. (2001) Two-state allosteric behavior in a single-domain signaling protein, *Science 291*, 2429−2433.
67. Bode, W., Papamokos, E., and Musil, D. (1987) The high-resolution X-ray crystal structure of the complex formed between subtilisin Carlsberg and eglin c, an elastase inhibitor from the leech Hirudo medicinalis. Structural analysis, subtilisin structure and interface geometry, *Eur. J. Biochem. 166*, 673−692.
68. Koradi, R., Billeter, M., and Wuthrich, K. (1996) MOLMOL: a program for the visualization and analysis of macromolecular structures, *J. Mol. Graphics 14*, 51−55.
69. Christopher, J. A., Swanson, R., and Baldwin, T. O. (1996) Algorithms for finding the axis of a helix: fast rotational and parametric least-squares methods, *Comput. Chem. 20*, 339−345.

BI0494424